Wind-Tunnel Wall Interference Effects on a Supercritical Airfoil at Transonic Speeds

James A. Blackwell Jr.* and Gerald A. Pounds†
Lockheed-Georgia Company, Marietta, Ga.

Wind-tunnel tests of a 10% supercritical airfoil have been conducted at transonic speeds in the Lockheed Compressible Flow Facility to determine the effects of varying wind-tunnel wall porosity on airfoil performance. Wall configurations ranging in porosity from 1.3 to 10% were investigated at Reynolds numbers of 7×10^6 to 30×10^6. Experimental data, which are presented to show the effects of varying wall porosity, include airfoil surface pressures, airfoil forces, and wind-tunnel wall pressures. Utilizing the experimental results, an assessment of the applicability of current subcritical theoretical methods to predict wall interference corrections in subsonic and transonic flows is made.

Nomenclature

C_p = pressure coefficient
c = chord of airfoil, in.
c_d = section profile drag coefficient
c_m = section pitching-moment coefficient about quarter-chord
c_n = section normal force coefficient
c_{n_α} = normal force vs angle-of-attack curve slope ($dc_n/d\alpha$), deg^{-1}
M = freestream Mach number
ΔM = Mach number correction due to wind-tunnel wall interference
R = wall resistance factor
RN = Reynolds number based on freestream conditions and airfoil chord
x = ordinate along airfoil chord line measured from airfoil leading edge, in.
z = ordinate vertical to airfoil chord line, in.
α = airfoil angle of incidence, deg
α_D = airfoil geometric angle of attack which approximately yields c_{n_D} at the design Mach number of 0.80, deg
$\Delta\alpha_c$ = angle-of-attack correction due to wind-tunnel wall interference, deg
τ = tunnel wall porosity (open area/closed area), %

Subscripts

B = blockage
D = design
s = shock location

Introduction

CURRENTLY, no general method for calculating wall interference corrections in conventional wind tunnels at transonic speeds is available. Thus, the use of subcritical flow theory has been the accepted means of determining wall interference corrections even at transonic speeds. The magnitude of the inaccuracies that occur when subcritical methods are used at transonic speeds is not generally known.

To provide additional insight into the subject of wind-tunnel wall interference, the Lockheed-Georgia Company has tested a 10% thick supercritical airfoil at transonic speeds over a wide range of wall geometries in the Lockheed Compressible Flow Facility (CFF). In particular, wall configurations ranging in porosity from near closed to 10% open have been investigated at Reynolds numbers of 7×10^6 to 30×10^6.

The purpose of this paper is to summarize the significant results of this investigation. Specific objectives will be to 1) quantify the magnitude of the experimental effects on aerodynamic performance resulting from varying wind-tunnel wall porosity; 2) assess the applicability of available subcritical methods to correct experimental data at transonic speeds for wall interference effects; and 3) provide additional understanding and insight into wall interference phenomena.

Experimental Tests

Test Facility

The Lockheed-Georgia Compressible Flow Facility is a blowdown wind tunnel capable of operating at Mach numbers from 0.20 to 1.20. The stagnation pressure can be varied from 20 to 175 psia, which results in a capability of simulating Reynolds numbers from those of conventional transonic wind tunnels to those near full-scale flight values (RN range approximately 6×10^6 to 55×10^6/ft at $M=0.80$). The test section, with the airfoil model installed, is shown in Fig. 1.

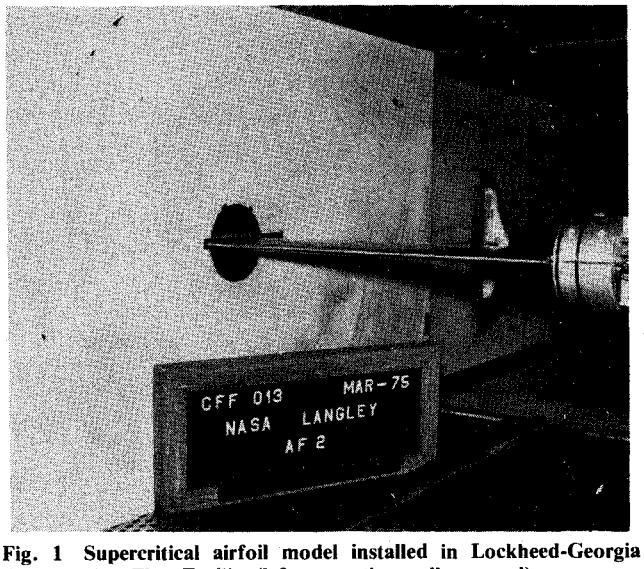

Fig. 1 Supercritical airfoil model installed in Lockheed-Georgia Compressible Flow Facility (left test section wall removed).

Presented at the AIAA 9th Aerodynamic Testing Conference, Arlington, Texas, June 7-9, 1976 (in bound volume of Conference papers, no paper number); submitted July 22, 1976; revision received June 6, 1977.

Index categories: Testing, Flight and Ground; Subsonic Flow; Transonic Flow.

*Scientist. Member AIAA.

†Aircraft Research and Development Engineer, Senior. Member AIAA.

The test section is 20 in. wide × 28 in. high × 72 in. long. For two-dimensional airfoil tests, the test section consists of solid sidewalls and variable-porosity top and bottom walls. A complete description of the test facility may be found in Ref. 1. A fixed-wake survey rake for section drag measurements is shown installed in the tunnel in Fig. 1. The wake rake was mounted at the tunnel centerline one chord length behind the airfoil model.

Static pressure orifices were installed in the left tunnel sidewall and in pressure rails (Fig. 1) on the tunnel floor and ceiling. The pressure rails were used to measure the flowfield as close to the tunnel floor and ceiling as possible, without interference from the porous wall. The pressure rails were mounted on the wind-tunnel floor and ceiling midway between the tunnel sidewalls. The rail design was patterned after the installation used for similar measurements in Ref. 2.

The variable-porosity top and bottom test section walls consist of two adjacent perforated plates with 0.25-in.-diam holes slanted 60° from the vertical. The porosity of the wall may be varied from closed to 10% open by moving the outside shutter plate upstream to misalign the perforations.

Model

The two-dimensional model used in this investigation is a NASA 10% supercritical airfoil design. The model has a chord of 7 in. and completely spans the test section. Surface pressure orifices were installed near the midspan region of the model on the upper and lower surfaces to provide for measurement of the chordwise distribution of pressures.

Test Techniques

The airfoil section normal force and pitching-moment coefficients were computed by integration of the chordwise pressure distributions. Section profile drag data were computed from the wake survey rake measurements by the method of Ref. 3.

Presentation of Experimental Results

The effects of wall porosity variations were obtained on all important aerodynamic parameters, such as airfoil normal force, drag, and pitching moment; airfoil surface pressures; and wind-tunnel wall pressures. Presentation of the results in this paper will be limited to data for the design normal force coefficient and the design geometric angle of attack. The experimental data in this paper generally will be denoted by line symbols rather than point symbols to illustrate the pertinent aerodynamic effects better. Also, the presentation of results other than pressure data will be in incremental form, with results for a wind-tunnel wall porosity of 4% used as datum unless otherwise specified.

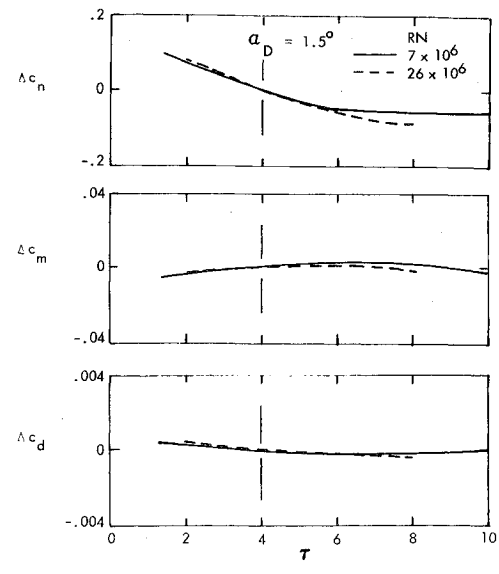

a) $M = 0.60$

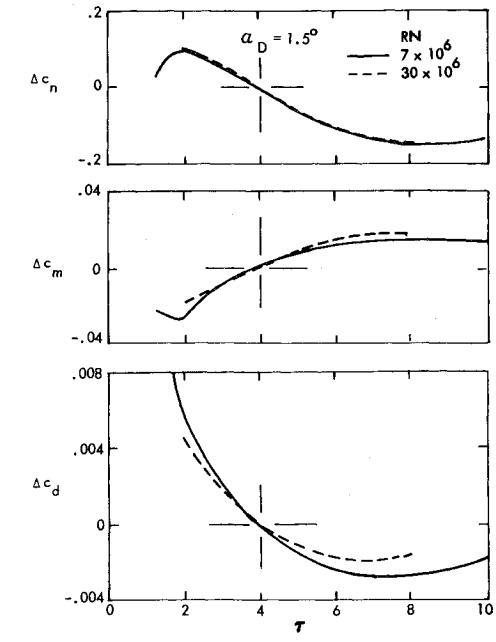

b) $M = 0.80$

Fig. 2 Variation of force data with τ at design angle of attack.

Discussion of Results

Force Characteristics

The basic force characteristics at the design angle are summarized with respect to variations in wall porosity in Fig. 2 for both subcritical and supercritical Mach numbers. The effect of increasing wall porosity can be seen to result in a decrease of the normal force coefficient. This reduction in normal force is due to the progressive changes in effective angle of attack of the airfoil resulting from the induced flow angularity produced by the walls. The rate at which the normal force is reduced also varies with porosity. The effect of porosity variations on the pitching-moment coefficient is small at subsonic speeds but significant at transonic speeds. The large changes in pitching moment seen for $M = 0.80$ are due to substantial movements of the shock on the airfoil (see Fig. 5b). The variation of drag coefficient with porosity at $M = 0.60$ is small relative to that shown for $M = 0.80$. The overall change in drag coefficient at $M = 0.80$ is approximately 0.0229 over the porosity range tested (1.3 to 10%). This large change in drag coefficient at transonic speeds is a result of substantial variations in the airfoil pressure distributions (to be presented later), resulting from both the normal force reductions due to the changes in effective angle of attack and the influence of porosity on the Mach number (blockage).

The influence of Reynolds number on the variation of the force data with wall porosity changes is also shown in Fig. 2. The trends of the force data with porosity are seen to be generally the same for both low and high Reynolds number data. As can be seen, Reynolds number has little influence on porosity effects. The differences noted in the drag data of $M = 0.80$ are attributed primarily to the sensitivity of the airfoil to slight changes in Mach number, since for the lower values of porosity the airfoil is well into the drag-rise (see Fig. 4).

The variation of the force characteristics with porosity at the design normal force is presented in Fig. 3. By comparing the force data at a constant normal force coefficient, the induced angularity effect of the porous walls (as indicated by linear theory) is effectively neutralized. Therefore, the variations in forces shown in Fig. 3 should be those directly associated with other wall interference effects, such as blockage. As can be seen, the induced flow angularity effect due to wall porosity is quite large. It is also of interest to note that the induced flow angularity is nearly the same for both

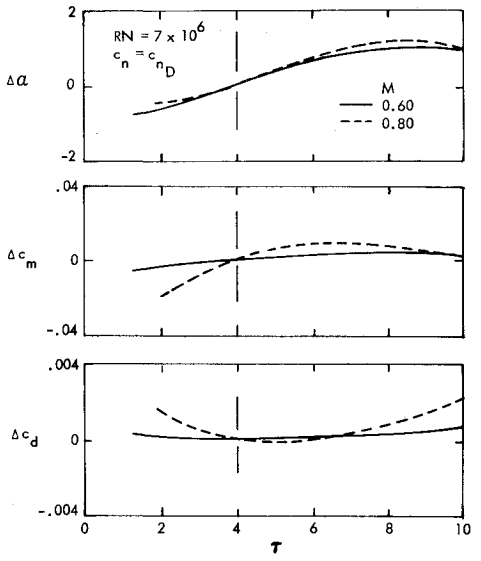

Fig. 3 Variation of force data with τ at design normal force coefficient.

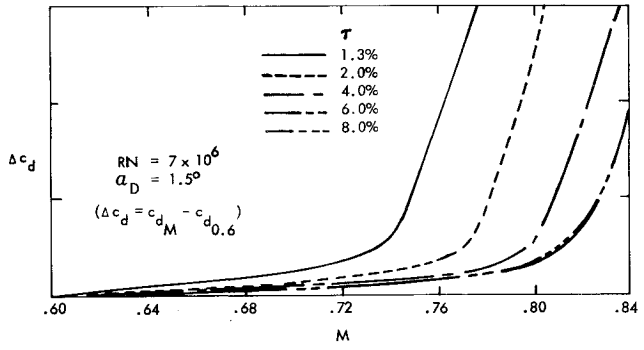

Fig. 4 Variation of drag coefficient with Mach number at design angle of attack.

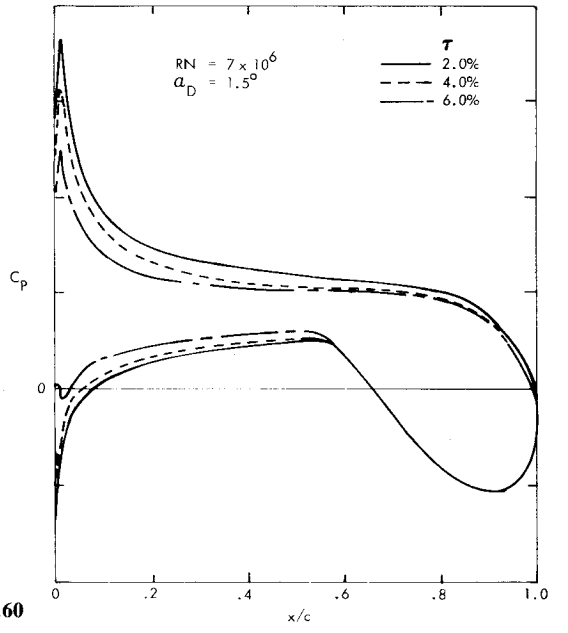

a) $M = 0.60$

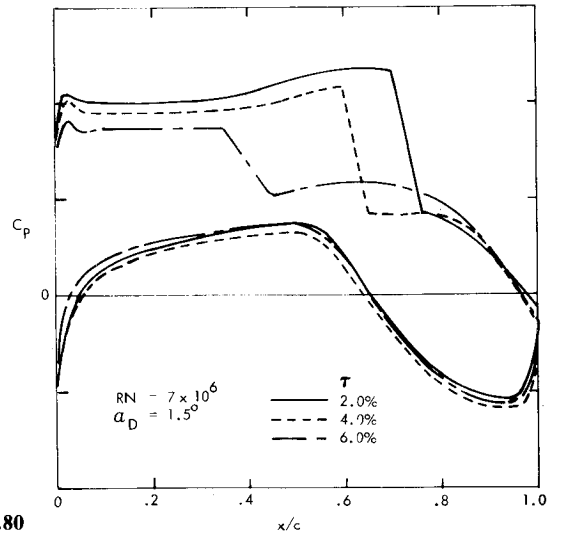

b) $M = 0.80$

Fig. 5 Variation of airfoil pressure distribution with τ at design angle of attack.

subcritical and supercritical speeds. At subsonic speeds, the variations of pitching moment and drag coefficient are similar to those shown in Fig. 2 for a constant angle of attack; i.e., the pitching-moment and the drag coefficient variation is small. At transonic speeds, large effects of porosity on the pitching moment and drag coefficients are indicated. As mentioned previously, these significant changes are associated with the large influence of wall porosity on the transonic pressure distributions.

In Fig. 4, the variation in airfoil drag coefficient is presented for selected wall porosities at the design angle of attack of 1.5°. It may be observed that large variations in airfoil drag-rise characteristics occur with porosity changes. Over the range of porosities investigated, a change of approximately 0.08 in drag-rise Mach number was experienced. This variation is caused primarily by both blockage effects and the change in airfoil normal force coefficient which accompanies the variation in porosity at constant geometric angle of attack. An analysis of the drag data indicates that the effect of the normal force reductions as porosity is increased results in approximately half the drag-rise Mach number variation shown in Fig. 4. Thus, the wall interference effects on the drag-rise Mach number at the design normal force coefficient is on the order of 0.04 in Mach number over the investigated porosity range.

Airfoil Surface Pressure Distribution

The effect of wind-tunnel wall porosity on the airfoil pressure distributions is shown in Fig. 5 at the design angle of attack of 1.5° for selected porosities. Subcritical wall interference theory[4] indicates that the variations in wall porosity result in changes in the effective flow angle and changes in the freestream Mach number. At subsonic speeds (Fig. 5a), the effect of wall porosity on the pressure distribution shape appears to follow closely that which would be expected primarily from a variation in effective flow angle. At transonic speeds (Fig. 5b), the effect of varying porosity on the pressure distribution is much larger than that shown for subsonic speeds. The variations at transonic speeds are similar to that which would be expected from either a change in angle of attack or freestream Mach number. However, from examination of this figure alone, it is difficult to assess what differences are caused by flow angle and what differences are attributable to the effects of wall porosity on freestream Mach number.

To neutralize the induced angularity effect of wall porosity on the airfoil pressure distributions, results are presented in Fig. 6 at the design normal force coefficient for selected porosities. At subsonic Mach numbers, a comparison of Figs. 5a and 6a indicates that the dominant effect of wall porosity is essentially effective flow angle change. A small effect of blockage on the subcritical pressures (Fig. 6a) can, however, be seen, as evidenced by the shift in the pressure distribution levels. At transonic speeds (Fig. 6b), analysis of the results at

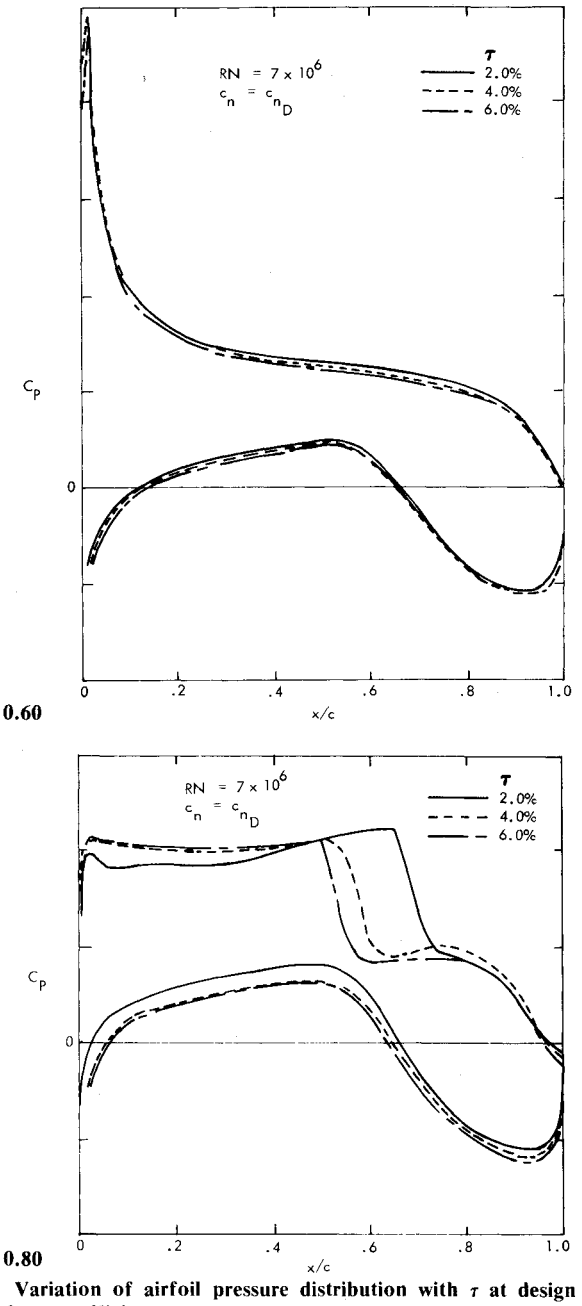

a) $M=0.60$

b) $M=0.80$

Fig. 6 Variation of airfoil pressure distribution with τ at design normal force coefficient.

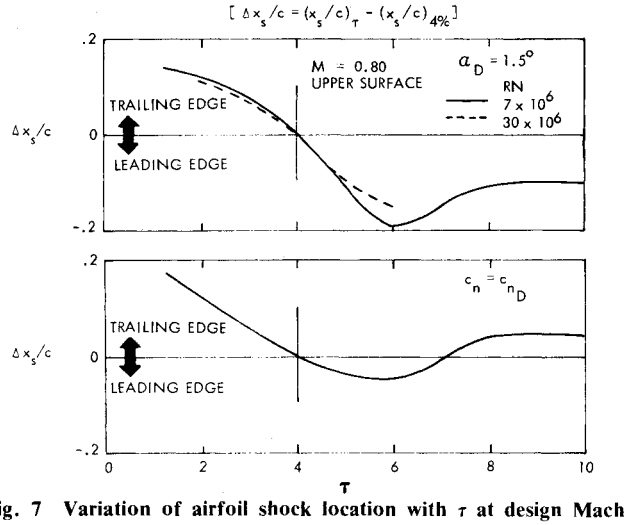

Fig. 7 Variation of airfoil shock location with τ at design Mach number.

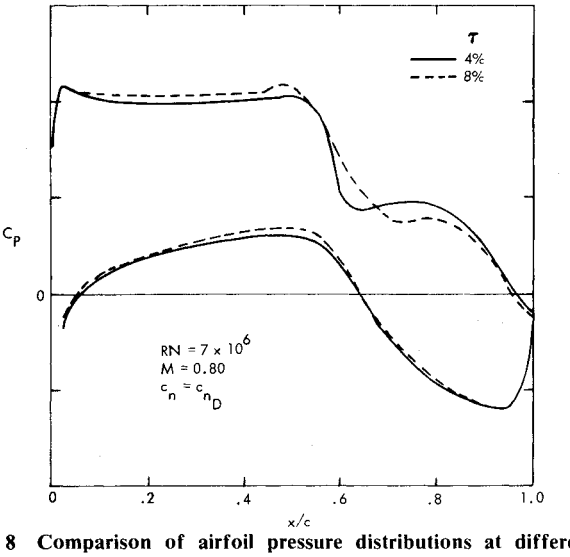

Fig. 8 Comparison of airfoil pressure distributions at different porosities with similar shock locations.

a constant normal force coefficient eliminates much of the large variation in the pressure distributions caused by changes in porosity shown in Fig. 5b. However, significant differences remain which probably are due to the effect of wind-tunnel wall porosity on blockage interference.

In Fig. 7, the movement of the airfoil upper-surface shock location at $M=0.80$ with variations in wall porosity is summarized. The shock location is defined as the point on the airfoil where the airfoil pressure distribution crosses the value of pressure coefficient corresponding to a local Mach number of one. At the design angle of attack of 1.5°, the shock travel is approximately 32% of the airfoil chord. For the design normal force coefficient, the shock movement is approximately 22% of the airfoil chord over the range of wall porosities investigated.

In comparison, the effect of Reynolds number on shock location at the airfoil design conditions ($M=0.80$, $\alpha_D=1.5°$) and a wall porosity of 4% is only 3% of the airfoil chord for a Reynolds number variation of 4×10^6 to 32×10^6. Thus, it is evident that at the design conditions the effect of wall porosity is much greater than the effect of Reynolds number. The influence of Reynolds number on the effect of wall porosity on the airfoil pressures also is indicated in Fig. 7 by presenting the airfoil upper-surface shock movement as a function of wall porosity for chord Reynolds numbers of 7×10^6 and 30×10^6 at $M=0.80$. As observed, the influence of Reynolds number on wall porosity effects is small.

The curve in Fig. 7 for constant normal force coefficient illustrates an interesting property. There are two wind-tunnel wall porosities that yield the same value of shock location. This might imply that the blockage effect on Mach number is the same for the two values of porosity. Accordingly, the airfoil surface pressures at the design normal force coefficient were plotted in Fig. 8 for two porosities with approximately the same shock locations: 4 and 8%. As can be seen, the pressure distributions agree very well except in the vicinity of the shock. The shock for 8% porosity is smeared over a considerably longer chordwise extent relative to the shock for 4% porosity.

To determine the magnitude of the wall interference effect on Mach number, data at 2 and 4% porosities were compared at the design normal force coefficient for conditions where the shock occurred at the same chordwise location. The wind-tunnel data were acquired at a freestream Mach number of 0.796 for the 2% porosity data and 0.817 for the 4% porosity data. The 2% data are shown in Fig. 9 corrected to $M=0.817$ using an assumed Mach number correction of +0.021. The

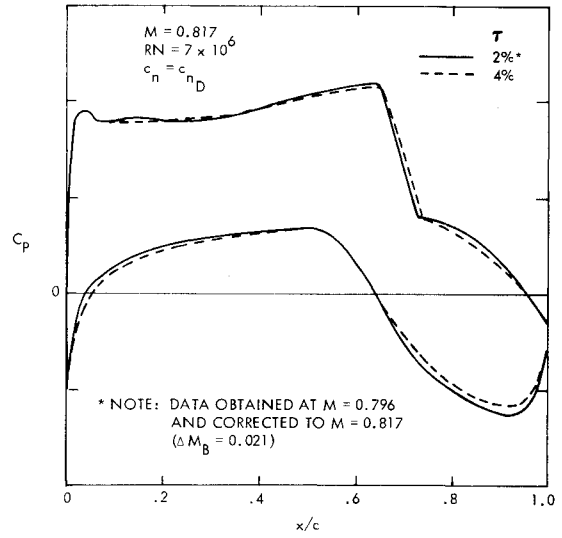

Fig. 9 Comparison of airfoil pressure distributions corrected for blockage effect on Mach number.

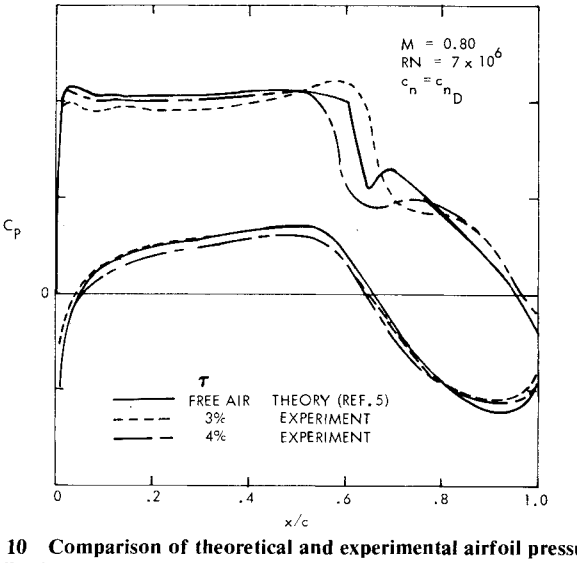

Fig. 10 Comparison of theoretical and experimental airfoil pressure distributions.

agreement between the 4% data and the corrected 2% data is very good. The agreement is significantly improved relative to the uncorrected comparison presented in Fig. 6b. The good agreement indicates that the blockage effect on Mach number is of the assumed order of magnitude. This assumed value is considerably larger than the blockage effect calculated by linear theory,[4] which yields a correction of approximately 0.004 in Mach number.

A comparison similar to that in Fig. 9 was made for each of the porosities investigated at $c_n = c_{n_D}$ and $M = 0.80$ to determine the maximum Mach number correction that would be required to collapse the data. These comparisons indicated that the blockage effect on Mach number due to varying wall porosity from 1.27 to 9.96% was on the order of 0.04. It is interesting to note that this increment is the same as that observed earlier in the variation of drag-rise Mach number with porosity at a constant design normal force coefficient.

In Fig. 10, a comparison of the experimental airfoil pressure distributions at $M = 0.80$ and $c_n = c_{n_D}$ is made with theoretical results in free air using the viscous transonic program of Ref. 5 with the nonconservative differencing scheme. Of the porosities investigated, the experimental data for 3 and 4% porosity agree best with the theoretical free-air results.

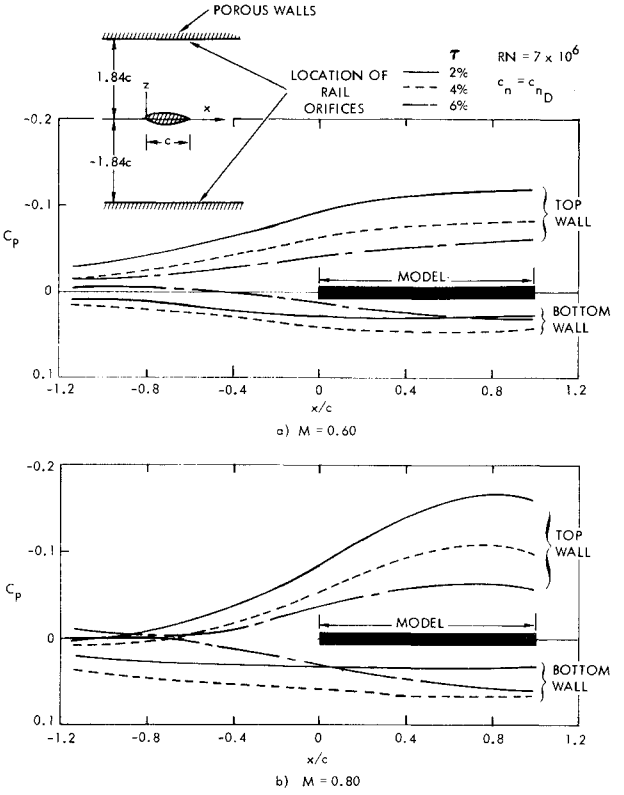

Fig. 11 Variation of wall pressure distributions with τ at design normal force coefficient.

Wind-Tunnel Wall and Rail Pressure Distributions

The rail pressure distributions in Fig. 11 show considerable variations with wall porosity. In terms of Mach number, the rail results show a progressive decrease in local Mach number at the top wall as porosity is increased from 2 to 6%. At the bottom wall, the local Mach number also decreases as porosity increases from 2 to 4%, but at 6% the trend reverses, and the local Mach number begins to increase again. Since the normal force is constant, this would indicate that a blockage effect on Mach number is present and is varying with wall porosity. It also should be noted that the rail pressures at $M = 0.80$ are considerably below the critical speed such that the wall flow is entirely subcritical.

The effect of wall porosity on the wind-tunnel wall pressures at various vertical locations above the airfoil model is illustrated in Fig. 12, where the experimental sonic line locations are shown at $M = 0.80$. As porosity is increased (at constant design normal force), the chordwise extent of the sonic line is reduced consistent with the movement of the airfoil shock wave noted earlier. The crest of the supersonic zone occurs at approximately one-half chord above the airfoil surface, which is considerably below the ceiling wall ($z = 1.84c$). The similarity of the sonic line shape near the airfoil for the 4 and 8% porosity data is consistent with the pressure distribution agreement previously presented in Fig. 8. The small differences in the airfoil surface pressures occur even though there are large differences between the 4 and 8% porosity pressure data on the wind-tunnel top and bottom walls (Fig. 13). The theoretical sonic line in free air as computed from Ref. 5 also is presented in Fig. 12. Notable differences exist between the theoretical and experimental sonic lines.

Analysis of Subcritical Wall Corrections

An analysis was performed to see if some insight could be gained in determining the suitability as well as the range of applicability of subcritical wall correction methods for correcting subsonic and transonic flows. Two methods were considered. The first is the conventional AGARD subcritical

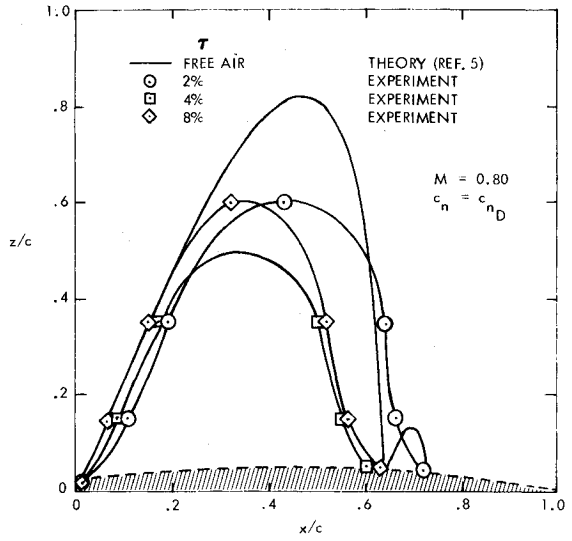

Fig. 12 Comparison of theoretical and experimental sonic-line locations at design conditions.

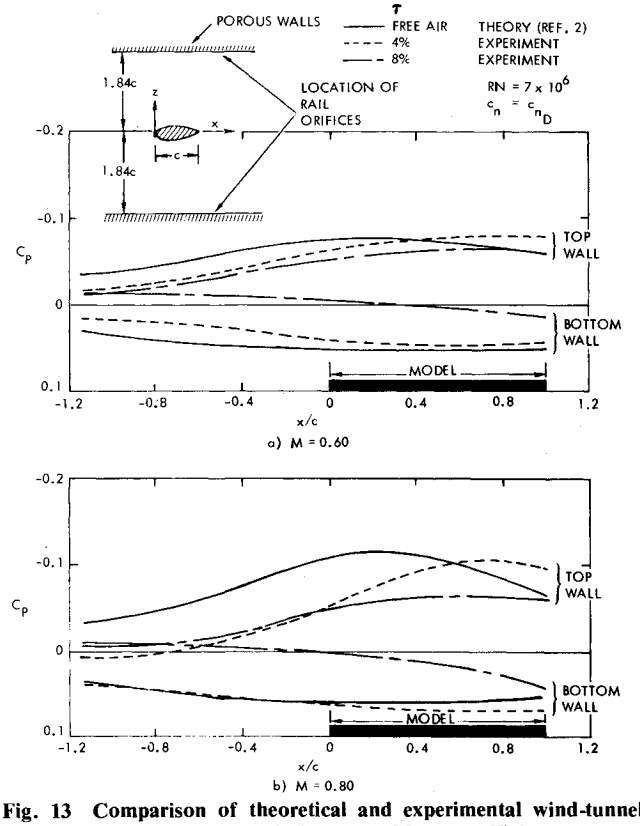

Fig. 13 Comparison of theoretical and experimental wind-tunnel wall pressure distributions at design normal force coefficient.

wall interference correction method of Ref. 4. This approach assumes that the wall resistance factors R are the same on the top and bottom wind-tunnel walls. Values of R for the various wall porosities were determined from previous investigations in the CFF and are recorded in Ref. 6.

A second method has been developed at the National Aeronautical Establishment (NAE)[2] which allows a differential wall resistance factor between the top and bottom walls. This method is based on the observation that the individual tunnel walls may have different resistances to the flow, depending on whether they are experiencing inflow from the plenum chamber into the test section or outflow from the tunnel test section into the plenum chamber. The resistance factors for each wall are determined by matching

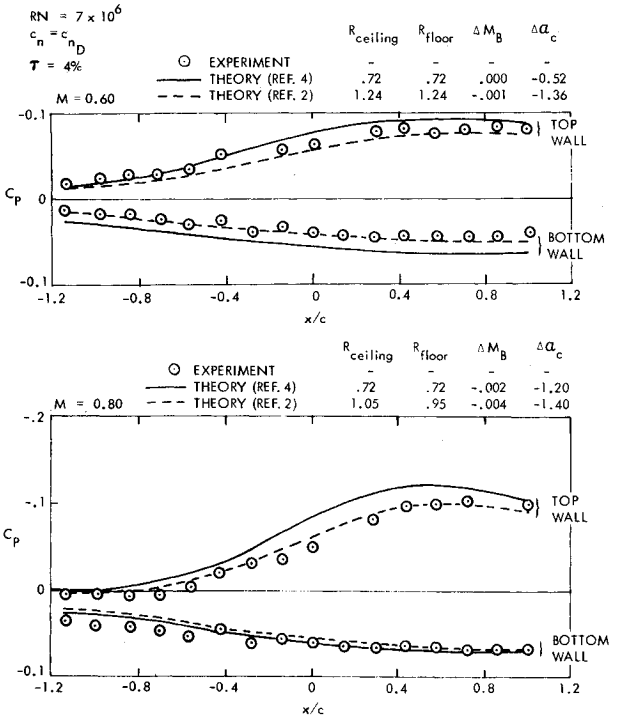

Fig. 14 Comparison of theoretical wall pressure distributions with experiment at design normal force coefficient.

the theoretical wall (ceiling and floor) pressure distributions with the experimental data.

The theoretical pressure distributions[2,4] at the tunnel floor and ceiling have been computed and compared to the experimental rail pressure data over a wide range of flow conditions and wall porosities. An example of this correlation is presented in Fig. 14 for a wall porosity of 4%. The use of a constant resistance factor[4] as determined from Ref. 6 ($R = 0.72$) gives a reasonable agreement between experiment and theory. It should be pointed out, however, that, of the comparisons made using the conventional correction theory of Ref. 4, the one presented in Fig. 14 is by far the best. Use of Ref. 2 to calculate the wall pressures, where the top and bottom resistance factors are allowed to float to obtain a close match between theory and experiment, results in a good correlation with the experimental rail pressures. This remains true for transonic speeds up to the design Mach number.

The corrections to Mach number and angle of attack as calculated from the two methods[2,4] are presented for a range of wall porosities in Fig. 15. As can be seen, the wall matching corrections yield Mach number corrections significantly larger than the conventional corrections. The conventional correction has only one value of porosity which yields zero blockage, whereas the wall matching correction has two values over the porosity range investigated. The experimental results in Fig. 8 implied that there are two values of porosity which yield the same blockage correction. In addition, the variation with porosity of the wall matching blockage corrections appears to be of the correct order of magnitude, whereas the conventional corrections are not. For example, the Mach number difference required to collapse the 2 and 4% porosity pressure data in Fig. 9 (i.e., $\Delta M_B = 0.021$) compares to a theoretical difference of 0.015 in Fig. 15 for the wall matching method. The porosities for zero blockage using the wall matching method cannot be predicted accurately at this time; however, the results in Fig. 10 indicate that the best correlation of free-air theoretical results with experimental data is achieved using experimental data at the porosities predicted for zero blockage correction in Fig. 14b. Thus, it appears that the method of Ref. 2 shows considerable promise for calculating the model blockage effect on Mach number. The corrections to angle of attack (Fig. 15) from the

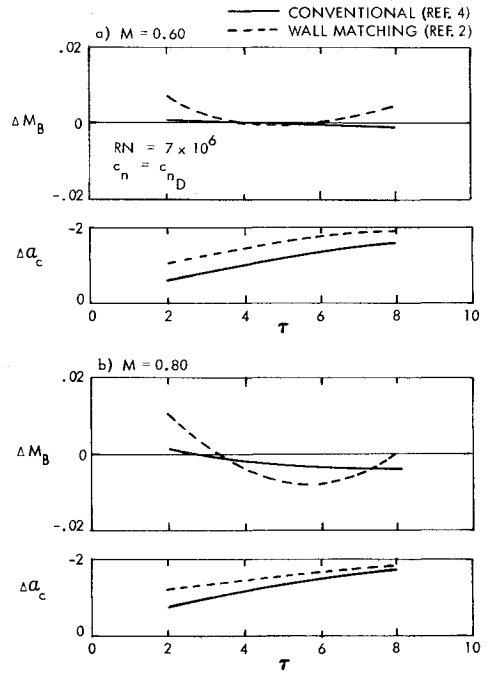

Fig. 15 Theoretical wall interference corrections at design normal force coefficient.

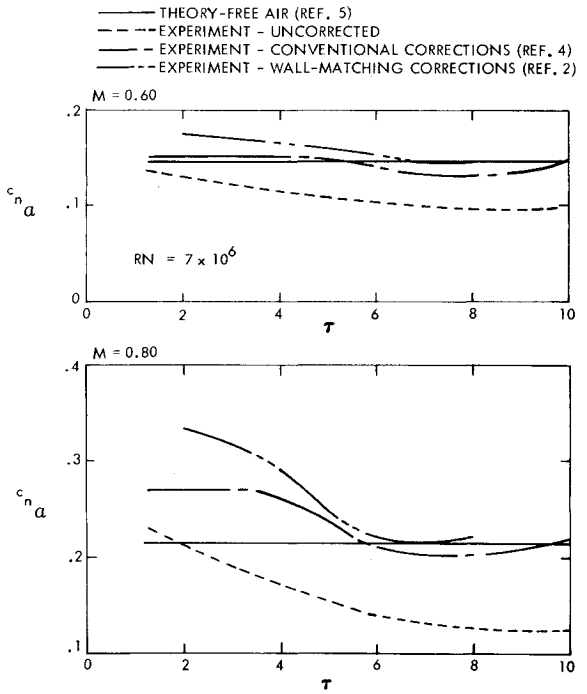

Fig. 16 Comparison of experimental and theoretical normal force vs angle-of-attack curve slope with τ.

two methods are consistent in trend with the wall matching method yielding the largest corrections.

To determine some measure of the accuracy of the two methods to predict the angle-of-attack corrections, the experimental geometric angle-of-attack data have been corrected, and the resulting normal force vs angle-of-attack curve slopes have been compared to results calculated by the viscous transonic theory (free air) of Ref. 5. The results of this correlation are illustrated in Fig. 16. The use of the conventional method to correct the experimental normal force curve slopes at subsonic speeds produces a uniform normal force curve slope over the porosity range of 1.3 to 4%, which is in good agreement with the theoretical viscous free-air solution. At transonic speeds, a uniform slope is produced, but the magnitude is significantly in error. The experimental data corrected using the wall matching method do not produce a uniformly corrected normal force curve slope at either subsonic or transonic speeds.

Concluding Remarks

The results from a wind-tunnel test on a 10% thick supercritical airfoil have been presented for wind-tunnel wall porosities varying from 1.3 to 10% at Mach numbers of 0.6 and 0.8 and at Reynolds numbers of 7×10^6 and 26 to 30×10^6. The experimental results have been compared to transonic theoretical predictions in free air to determine interference-free conditions and to assess the applicability of current subcritical wall-interference correction methods. Analysis of these results has produced the following concluding remarks:

1) The effect of changes in wind-tunnel wall geometry through varying test section wall porosity on the airfoil aerodynamic performance is significantly larger at transonic speeds than for subsonic speeds.

2) A comparison of the variations in the aerodynamic data with wall porosity for both low (7×10^6) and high (26 to 30×10^6) Reynolds number conditions indicates that the effect of Reynolds number on porosity effects is small.

3) At the airfoil design conditions of $M=0.80$ and geometric angle of attack of 1.5°, the maximum variations in the airfoil aerodynamics due to increasing wall porosity from 1.3 to 10% were a normal force coefficient decrease of 0.25, a drag coefficient decrease of 0.0229, a drag-rise Mach number increase of 0.08, and an airfoil upper surface shock location movement of 32% chord.

4) Conventional subcritical AGARD wind-tunnel wall corrections for Mach number and angle of attack are generally inadequate for use at subsonic or transonic speeds, with the only exception being the adequacy of angle-of-attack correction at subsonic speeds below 4% porosity. The subcritical NAE wall matching method appears to yield reasonable Mach number corrections at both subsonic and transonic speeds. The angle-of-attack correction does not appear to be uniformly applicable over the range of wall porosities investigated.

5) When the proper angle-of-attack and Mach number wall interference corrections were known and applied to the data, the porous wall interference effects generally were neutralized.

6) A significant difference in the far-field pressure distributions above and below the airfoil can occur at transonic speeds without seriously affecting the measured airfoil characteristics.

Acknowledgment

The experimental work reported in this paper was sponsored by the NASA Langley Research Center under Contract NAS1-12325 with the Lockheed-Georgia Company.

References

[1]Pounds, G. A. and Stanewsky, E., "The Research Compressible Flow Facility," Lockheed-Georgia Co., ER-9219, 1967.

[2]Mokry, M. L., Peake, D. J., and Bowker, A. J., "Wall Interference on Two-Dimensional Supercritical Airfoils, Using Wall Pressure Measurements to Determine the Porosity Factors for Tunnel Floor and Ceiling," National Aeronautical Establishment, LR-575, 1974.

[3]Pankhurst, R. C. and Holder, D. W., *Wind Tunnel Technique*, Sir Issac Pitman and Sons, Ltd., London, 1965, p. 276.

[4]Garner, H. C., Rogers, E.W.E., Acum, W.E.A., and Maskell, E. C., *Subsonic Wind Tunnel Wall Corrections*, AGARDograph 109, 1966.

[5]Bauer, F., Garabedian, P., Korn, D., and Jameson, A., *Supercritical Wing Sections II*, Springer-Verlag, New York, 1975.

[6]Pounds, G. A., "An Initial Two-Dimensional Wall Interference Investigation in a Transonic Wind Tunnel with Variable Porosity Test Section Walls," AIAA Paper 72-1011, Sept. 1972.